Incorporating AC Power Flow into the Multi-Energy System Optimization Framework COMANDO

Philipp Glücker*,†, Marco Langiu*,§, Thiemo Pesch*, Manuel Dahmen* and Andrea Benigni*,†,‡

*Forschungszentrum Jülich GmbH, Institute of Energy and Climate Research,
IEK-10: Energy Systems Engineering, Jülich 52425, Germany
†RWTH Aachen University, Aachen 52056, Germany
§RWTH Aachen University, Process Systems Engineering (AVT, SVT), Aachen 52056, Germany
‡JARA-Energy, Jülich 52425, Germany

Correspondence: p.gluecker@fz-juelich.de

***Abstract*—Most multi-energy system (MES) optimization frameworks employ a single- or multi-node approach for balancing the respective commodities and do not accurately represent the physical behavior of energy grids that exert a major impact on optimal MES design and operation. This paper presents the integration of power flow equations into our open-source energy system optimization framework COMANDO. To this end, three power grid representations are implemented, including the nonlinear AC power flow equations. In an illustrative case study, we compare the optimal design of a small MES with integrated AC power flow equations to the design resulting from the conventional single-node approach. In both cases we consider operation with intertemporal constraints. The results exemplify that accounting for AC power flow can significantly impact both the sizing of energy system components and the system operation.**

***Index Terms*—multi-energy system, optimization, load flow, power grids, reactive power control**

I. Introduction

In recent years, research focus has shifted towards the integration of different energy commodities into multi-energy systems (MESs), as such systems have shown huge potential to improve the economical, technical and environmental performance compared to their independent counterparts at both the design and operational level [1]. MES optimization frameworks mostly aggregate the grid to one or few nodes per commodity at which demand and generation are balanced. Such aggregation is applied to large-scale MESs (see, e.g., [2]–[5]) as well as microgrids (see, e.g., [6], [7]). This simplification is in stark contrast to power flow equations that model the flow of electric power between grid nodes in an interlinked system. Solving the power flow equations under consideration of the optimal system state while satisfying grid constraints such as limits for transmission lines, voltage magnitude, phase angle and reactive power generation is called optimal power flow (OPF) [8], [9]. To include the power flow formulation in design and operational optimization of MESs, the nonlinear power flow equations are typically simplified for computational tractability reasons, e.g., resulting in linear DC power flow equations in case of transmission grids (see, e.g., [10], [11]). Linearized power flow equations have also been combined with nonlinear AC power flow equations for energy system design and operation in a successive manner [12], i.e., the results of a first operational optimization with linearized power flows are given to MATPOWER [13], which subsequently solves the nonlinear AC power flow equations based on the Newton-Raphson algorithm. MATPOWER [13] is a MATLAB-based open-source project solely focusing on static AC and DC power flow simulations and their optimization. Similarly, the Python-based package Pandapower [14] targets modeling, analysis and optimization of power systems. PyPSA [15], another Python-based package, extends AC optimal power flow calculations to connected time series. Furthermore, it allows operational optimization of power grids coupled with other energy sectors. None of the mentioned tools, however, allows for MES design optimization.

In this paper, we integrate three different power grid modeling approaches, including the nonlinear AC power flow equations, into our open-source energy system optimization framework COMANDO to enable MES design optimization and operation considering power grid restrictions. COMANDO is a component-based MES optimization tool that allows flexible modeling using nonlinear and differential-algebraic equations [16]. The integration of AC power flow equations into the optimization framework is achieved by introducing a new electric bus model, a new generic branch model to represent cables, power lines or transformers, and by making some minor adjustments to existing component models as outlined in Section II.

In Section II, we further describe the power grid modeling within COMANDO. In Section III, we consider an illustrative case study to demonstrate MES design optimization based on AC power flow equations under consideration of intertemporal constraints. By comparing the obtained optimal design to a

This work was funded by the Helmholtz Association of German Research Centers through program-oriented funding and the Innovation Pool project "Energiewende und Kreislaufwirtschaft".

design resulting from the conventional single-node approach, we highlight the effects grid restrictions can exert on the sizing of components and the operational strategy. Section IV concludes our work.

II. Power grid modeling

Apart from the strongly simplifying single-node approach, electric power systems can be represented as networks of buses which are connected by branches, e.g., cables, transmission lines or transformers. Within the COMANDO framework, we implemented electric buses as subsystems of the overall system to which the relevant electrical components are added. Each branch is represented as a component that receives two connected buses as inputs. The branches contribute flow terms to the balance equations at each bus. One or several energy system components are connected to each bus. The overall power system thus consists of electric buses and the interconnecting branches.

There are various formulations for modeling power flow [17], also known as load flow, of which we implemented both the AC and the DC power flow in the branch flow formulation as well as the network transfer capacity (NTC) representation. The NTC approach represents a simple multi-node model which limits the power transfer between two nodes via branches. It is often utilized to plan the power flow between market areas within transmission networks [18]. However, it does not represent the natural power flow given by the ratio of the admittances as the NTC branches are solely characterized by capacity limits. The DC power flow linearizes the AC power flow equations in (1) and (2) by neglecting grid losses, assuming a uniform voltage level at all nodes and linearizing the sine and cosine terms using the small-angle approximation. The DC power flow equations approximate the real power transfer for transmission level networks quite precisely, while neglecting the reactive power flows [19].

For AC power flow, each electric bus has an associated voltage phasor which can be described by its magnitude U_i and phase angle θ_i. Similarly, the apparent power is a complex value described by the power angle φ_i. Its real and imaginary parts correspond to the active power P_i and the reactive power Q_i which are determined by the exchanged values of the connected components. The respective sign of P_i and Q_i determines whether power is injected or consumed. We incorporate the AC power flow equations in the branch flow formulation. The so-called generalized Π-branch model [9] is implemented, which can represent transmission lines, cables, and transformers. The transfer of active power P_ik and reactive power Q_ik across the branch connecting buses i and k is determined by [20]:

$$\begin{aligned} P_\mathrm{ik} = &\left(a_\mathrm{ik}U_\mathrm{i}\right)^2 g_\mathrm{ik} - a_\mathrm{ik}U_\mathrm{i}U_\mathrm{k}g_\mathrm{ik}\cos\left(\theta_\mathrm{ik}+\varphi_\mathrm{ik}\right) \\ &- a_\mathrm{ik}U_\mathrm{i}U_\mathrm{k}b_\mathrm{ik}\sin\left(\theta_\mathrm{ik}+\varphi_\mathrm{ik}\right) \end{aligned} \tag{1}$$

$$\begin{aligned} Q_\mathrm{ik} = &-\left(a_\mathrm{ik}U_\mathrm{i}\right)^2\left(b_\mathrm{ik}+\frac{b_\mathrm{ik}^\mathrm{sh}}{2}\right) + a_\mathrm{ik}U_\mathrm{i}U_\mathrm{k}b_\mathrm{ik}\cos\left(\theta_\mathrm{ik}+\varphi_\mathrm{ik}\right) \\ &- a_\mathrm{ik}U_\mathrm{i}U_\mathrm{k}g_\mathrm{ik}\sin\left(\theta_\mathrm{ik}+\varphi_\mathrm{ik}\right) \end{aligned} \tag{2}$$

In (1) and (2), $\theta_\mathrm{ik} = \theta_\mathrm{i} - \theta_\mathrm{k}$ represents the phase angle difference between two buses. Analogously, g_ik is the line conductance and b_ik is the line susceptance, $b_\mathrm{ik}^\mathrm{sh}$ is the shunt susceptance, a_ik and φ_ik represent the voltage tap ratio and tap changer phase shift of the transformer, with default values of $a_\mathrm{ik} = 1$ and $\varphi_\mathrm{ik} = 0$ for non-transformer branches. The quantities are described in the per-unit system, which expresses the electrical quantities as a ratio of the actual quantity to a reference value (see, e.g., [9]). The physical limitations of the power grid are included in the optimization problem as limits for the transferred current across the branches and as reactive power limits of the generators. Furthermore, the voltage magnitude is constrained within $0.9\,\mathrm{pu} \leq U_\mathrm{i} \leq 1.1\,\mathrm{pu}$ and the phase angle within $-30^\circ \leq \theta_\mathrm{i} \leq 30^\circ$ at each bus.

In order to implement the AC power flow equations within COMANDO, the quantities and equations for U, θ, P and Q are introduced, characterizing the electric bus model. Furthermore, existing component models are modified such that components that produce or consume active or reactive power contribute to the respective active and reactive power terms of the connected buses. At each electric bus, the active power and the reactive power are each balanced by an equality constraint consisting of the active and reactive power flow of the connected component and the respective flows assigned to each connected branch as formulated in (1) and (2).

III. Case study

Our case study is an illustrative multi-energy system with the commodities electricity, gas and heat, with the latter two being balanced via the single-node approach. A sketch of the MES including the single-line diagram of the 4-bus power system is shown in Fig. 1. Note that this case study does not fulfill the simplification requirements of the DC approach, which is only applicable to transmission networks. Furthermore, the NTC approach does not represent the natural load flow, but the power can choose its path independently within the branch capacity limits. For the power system representation, we therefore solely focus on the comparison between the conventional single-node approach and the newly integrated AC power flow formulation.

A. Setup

The MES contains two loads, namely a supercomputer (SC) connected at bus 2 and several office buildings which are connected at bus 4 at 400 V. Bus 4 is connected to the remaining system, which is operated at 10 kV, at bus 3 via a three-phase transformer. With the goal of enabling grid-isolated operation of the MES, a photovoltaic (PV) plant and a combined heat and power (CHP) plant should be built at bus 1 and 3, respectively. The thermal storage (TS) has a storage capacity of $E_\mathrm{max} = 1.30\,\mathrm{MWh}$ and the boiler (B) has a nominal output capacity of $P_\mathrm{nom} = 5.15\,\mathrm{MW}$. The underground cable between buses 1 and 2 has a current rating of $I_\mathrm{r} = 145\,\mathrm{A}$, whereas for the other two cables $I_\mathrm{r} = 320\,\mathrm{A}$. The ratio of electrical and heating power generation for the CHP plant varies with the part-load but cannot be adjusted

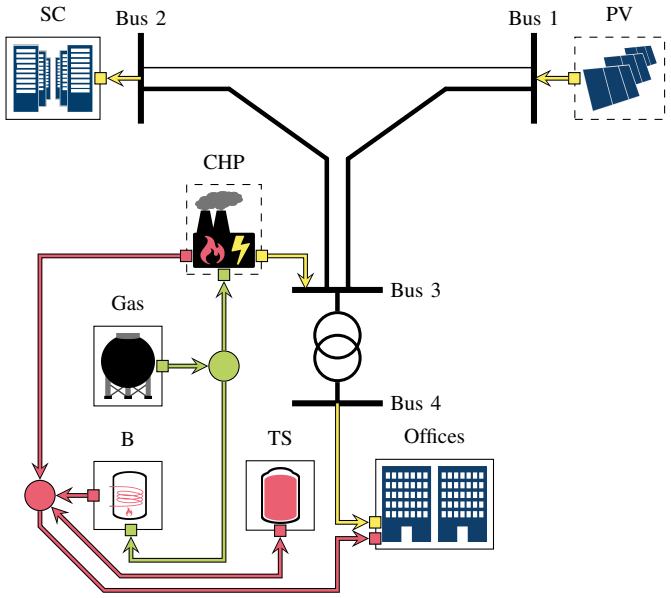

Figure 1. Multi-energy system including the commodities electricity (yellow), heat (red) and gas (green). A combined heat and power (CHP) plant and a photovoltaic (PV) array are to be installed and sized. Office buildings and a supercomputer (SC) must be supplied. A boiler (B) and a thermal storage (TS) already exist. The power grid consists of four buses with interconnecting branches, with a thinner cable between buses 1 and 2.

freely. Any excess of usable heat may be rejected via the exhaust of the CHP instead of being utilized.

Besides meeting the reactive power consumption of loads and branches, the supply of reactive power is responsible for keeping the node voltages within their operating range. As its transfer across large distances is not favorable, local reactive power supply is crucial for voltage stability [21]. In contrary to a local power plant control which controls the reactive power solely depending on the local voltage measurement, a centralized coordinated control considers the optimal operation of the whole MES for the reactive power supply [22]. Such systematic control approach will be an important task for future power grids, especially on the distribution level. In this case study, it is assumed that the CHP plant and the PV array are controlled by a centralized instance.

Depending on the system requirements, the two power plants can adjust their reactive power supply within a certain range of their power factor $\cos\varphi$, which is defined as the ratio of active power to apparent power. Subject to the respective active power generation at each time step, the range of the reactive power for the CHP plant and PV array are

$$-0.329\,P_{\mathrm{CHP}} \le Q_{\mathrm{CHP}} \le 0.75\,P_{\mathrm{CHP}}, \text{ and} \tag{3}$$

$$-0.484\,P_{\mathrm{PV}} \le Q_{\mathrm{PV}} \le 0.484\,P_{\mathrm{PV}}, \tag{4}$$

respectively, which are equivalent to the power factor range for the CHP plant of $\cos\varphi \in [0.95_{\mathrm{cap}}, 0.8_{\mathrm{ind}}]$ and for the PV array of $\cos\varphi \in [0.90_{\mathrm{cap}}, 0.90_{\mathrm{ind}}]$. Positive values represent injection and negative values represent consumption of inductive reactive power.

The supercomputer at bus 2 has a constant power demand, whereas the office buildings at bus 4 have a time-varying power and heat demand. The reactive power demand of the office buildings and the SC is determined dependent on the active power consumption such as $Q = 0.329P$, which is equivalent to a fixed power factor of $\cos\varphi = 0.95_{\mathrm{ind}}$. Heat demand and power demand profiles as well as the power factor (bounds) are based on aggregated data of comparable buildings on the campus of Forschungszentrum Jülich.

The year was clustered into eight representative days, with 24 time steps of a constant length of $\Delta\tau = 1\,\mathrm{h}$ per day and weights w_{d} accounting for the number of days assigned to each cluster. The solar irradiance used for the clustering is taken from [23] for the location Jülich, Germany, in the year 2019 based on [24]. Together with the days of maximum and minimum peak irradiance, the resulting ten representative days are used as operational scenarios in the design optimization. The objective of the design optimization is to determine the nominal size of the PV array (in $\mathrm{MW_{peak}}$) and the CHP plant (in $\mathrm{MW_{th}}$) in a cost-optimal manner. For this purpose, we consider the total annualized costs C_{TAC}, given as

$$C_{\mathrm{TAC}} = C_{\mathrm{I}}\, f_{\mathrm{ann}} + C_{\mathrm{fix}} + C_{\mathrm{var}}, \tag{5}$$

where the costs for overall investment (I), annual fixed (fix) and variable (var) operating costs are considered and f_{ann} represents an annualization factor of approximately 0.065/a, corresponding to an assumed lifetime of 30 years and an interest rate of 5%. The three cost terms are expressed as

$$C_{\mathrm{I}} = C_{\mathrm{ref}} \left(\frac{s}{1\,\mathrm{MW}}\right)^{0.9}, \tag{6}$$

$$C_{\mathrm{fix}} = c_{\mathrm{fix}}\, C_{\mathrm{I}}, \tag{7}$$

$$C_{\mathrm{var}} = c_{\mathrm{var}} \sum_d w_d \sum_t o_{d,t}\, \Delta\tau, \tag{8}$$

where for each component, s is the nominal size and $o_{d,t}$ is the value of an operational quantity for a given representative day d and time-step t. In the considered case study, the contributions according to (8) are from the CHP plant, the PV plant and the gas grid, with the operational quantity $o_{d,t}$ referring to the electrical output of the CHP plant and PV array, and the consumed amount of gas, respectively. The quantities C_{ref}, c_{fix}, and c_{var} have component-specific values, given in Tab. I.

Table I
COST COEFFICIENTS FOR THE COMPONENTS BOILER (B), COMBINED HEAT AND POWER (CHP) PLANT, GAS GRID (GAS) AND PHOTOVOLTAIC (PV) PLANT. NOTE THAT THE BOILER IS CONSIDERED TO BE PAID OFF AND ITS FIXED COSTS REFER TO ORIGINAL INVESTMENT COSTS OF 2.16 M€.

Component	C_{ref} [M€]	c_{fix} [%]	c_{var} [€/(MWh)]
B	-	1.4	0
CHP	1.183	3.5	1
Gas	-	0	45
PV	0.862	1.7	0.5

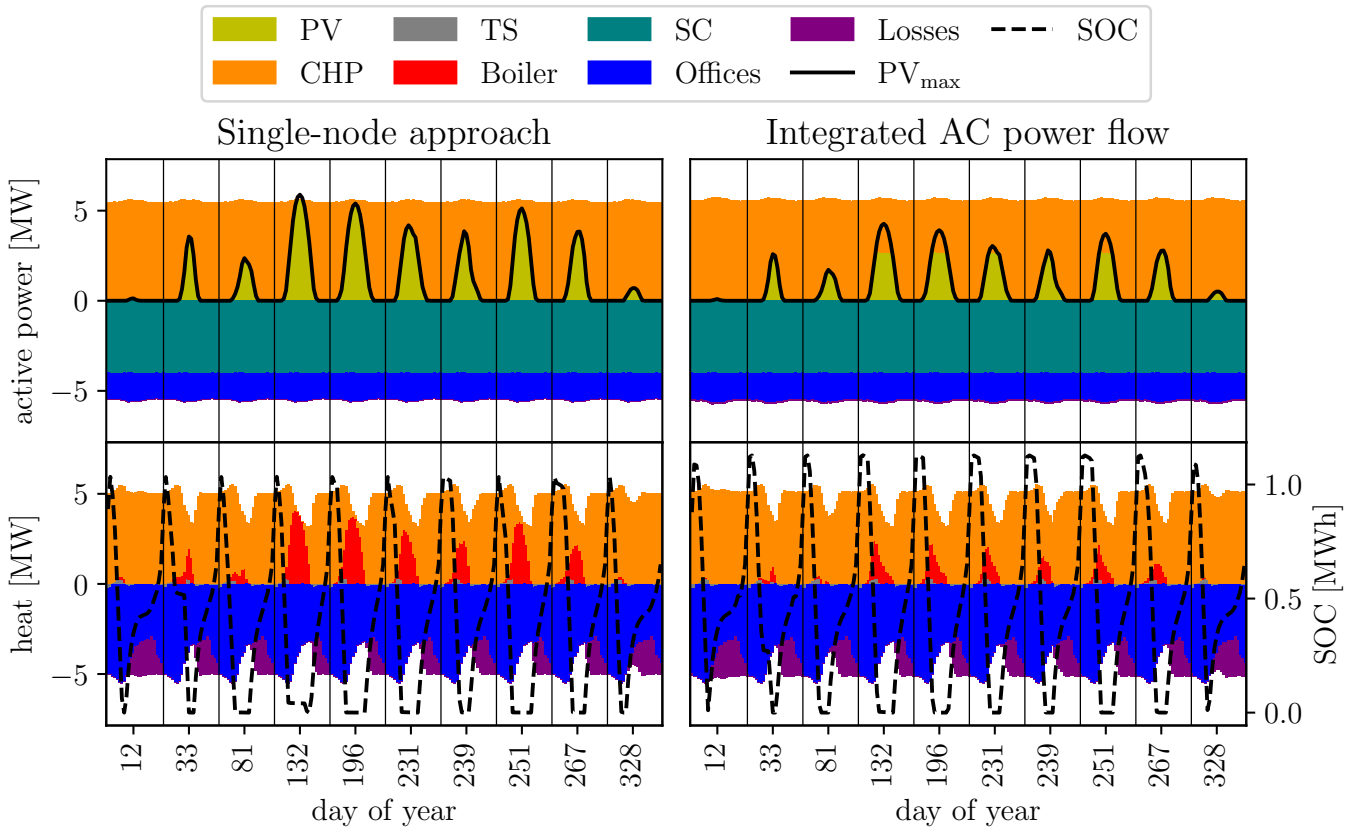

Figure 2. Results of the active power and the heat for the optimization with the single-node approach (left) and with the integrated AC power flow (right): Positive values represent generation and negative values represent demand for the photovoltaic (PV) array, combined heat and power (CHP) plant, thermal storage (TS), boiler, supercomputer (SC), office buildings (Offices) and losses. The active power is depicted together with the maximum possible PV ($\mathrm{PV}_{\max}$) output (top) and the heat is depicted together with the state of charge (SOC) of the thermal storage (bottom).

The problem formulation distinguishes between design and operational variables. The design variables are the size of the CHP plant, $P_{\max,\mathrm{CHP}}$, and of the PV array, $P_{\max,\mathrm{PV}}$. The operational variables are listed in Tab. II. The MES optimization model with integrated AC power flow equations has 19 operational variables per time step and per scenario, leading to a total of 4562 variables. All optimizations are performed on a 2.8 GHz Intel Core i7-4980HQ CPU with 16 GB of RAM using IPOPT 3.12 [25] with default settings.

B. Numerical results

The results displayed in Tab. III are local solutions. They were obtained in approximately 15 s for the single-node approach and 30 s for the AC power flow approach. It can be noted that the PV array is sized considerably larger in the single-node approach than with the AC power flow equations, whereas the CHP plant sizes match more closely.

The corresponding operational schedules for the ten representative days are shown in Fig. 2. Note that positive values correspond to supply and negative values to demands and losses, respectively. The active power from the larger PV array is completely used in the schedule of the single-node approach, apart from day 132 around noon where the generated power of the PV array slightly exceeds the power demand of the overall system. If the power grid is modeled with integrated power flow equations as shown in the right part of Fig. 2, the

Table II
OPERATIONAL VARIABLES FOR BOILER (B), COMBINED HEAT AND POWER (CHP) PLANT, GAS GRID (GAS), PHOTOVOLTAIC (PV) ARRAY, THERMAL STORAGE (TS) AND POWER GRID (PG). THE INDEX t DENOTES THE TIME STEP AND THE INDEX s DENOTES THE SCENARIO. NOTE THAT D_{gas} REPRESENTS THE QUANTITY OF GAS DEMANDED, $\dot{Q}$ STANDS FOR THE HEAT FLOW, WHEREAS Q REPRESENTS THE INJECTED REACTIVE POWER.

Component	Single-node	AC power flow
B	$\dot{Q}_{\mathrm{out,t,s}}$	$\dot{Q}_{\mathrm{out,t,s}}$
CHP	$\dot{Q}_{\mathrm{out,t,s}}$, $\dot{Q}_{\mathrm{heat\,sink,t,s}}$	$\dot{Q}_{\mathrm{out,t,s}}$, $\dot{Q}_{\mathrm{heat\,sink,t,s}}$, $Q_{\mathrm{t,s}}$
Gas	$D_{\mathrm{gas,t,s}}$	$D_{\mathrm{gas,t,s}}$
PV	$P_{\mathrm{t,s}}$	$P_{\mathrm{t,s}}$, $Q_{\mathrm{t,s}}$
TS	$SOC_{\mathrm{t,s}}$, $S\dot{O}C_{\mathrm{t,s}}$, $\dot{Q}_{\mathrm{in,t,s}}$, $\dot{Q}_{\mathrm{out,t,s}}$	$SOC_{\mathrm{t,s}}$, $S\dot{O}C_{\mathrm{t,s}}$, $\dot{Q}_{\mathrm{in,t,s}}$, $\dot{Q}_{\mathrm{out,t,s}}$
PG	–	$U_{\mathrm{B1,t,s}}$, $\theta_{\mathrm{B1,t,s}}$, $U_{\mathrm{B2,t,s}}$, $\theta_{\mathrm{B2,t,s}}$, $U_{\mathrm{B3,t,s}}$, $\theta_{\mathrm{B3,t,s}}$, $U_{\mathrm{B4,t,s}}$, $\theta_{\mathrm{B4,t,s}}$

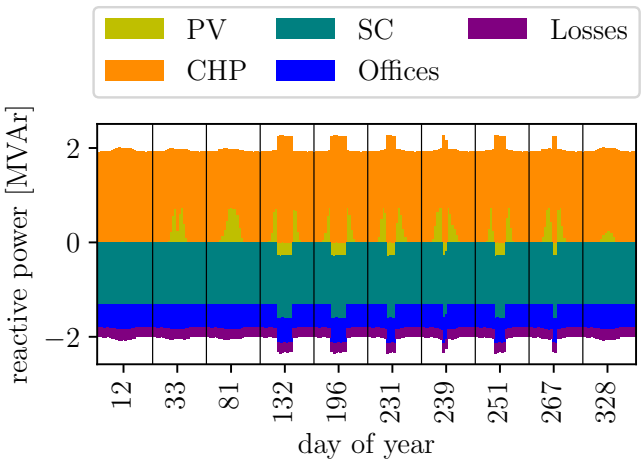

Figure 3. Results of the reactive power for the optimization with integrated AC power flow. Positive values represent generation and negative values represent consumption of inductive reactive power for the photovoltaic (PV) array, combined heat and power (CHP) plant, supercomputer (SC), office buildings (Offices) and losses.

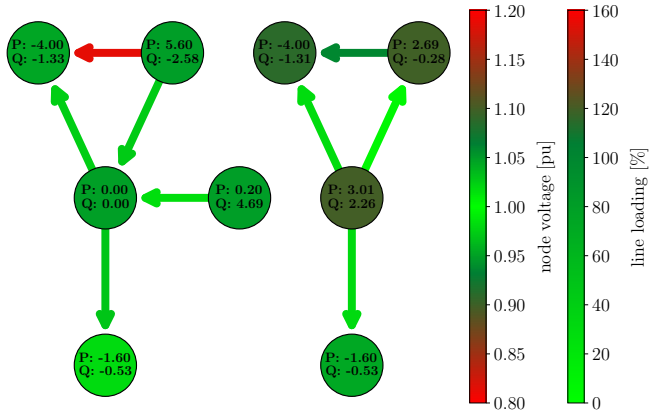

Figure 4. Line utilization and node voltages based on AC power flow in the hour of maximum solar input (day 132 at noon). Positive values represent generation and negative values represent consumption of direct power P (in MW) and inductive reactive power Q (in MVAr), respectively. Left: AC power flow based on the single-node design and operation. An additional slack bus supplies the losses of the power grid which are not considered in the single-node approach, as well as additional reactive power required to maintain the combined heat and power (CHP) plant and photovoltaic (PV) array within their limits for reactive power generation. Right: AC power flow based on the design and operation with integrated AC power flow equations.

PV output is curtailed during hours of high solar irradiance. The reason for this curtailment is the cable between buses 1 and 2 which would otherwise be overloaded due to the ratio of the respective branch admittances. Compared with the single-node approach, the optimization including the integrated AC power flow equations therefore results in a smaller designed PV array. The ohmic losses on the cables are included in the AC power flow equations as shown by the purple section in the top-right part of Fig. 2, in contrast to the single-node approach. The losses and the smaller sized PV array are the reasons for the slightly larger CHP design. Due to the higher feed-in of the PV array in the single-node design, the power and thus the heat output of the CHP is reduced during sunny days, leading to a more active boiler to supply the heat demand of the buildings.

The reactive power balance resulting from the optimization with integrated AC power flow equations is shown in Fig. 3. Once the limit of the cable between buses 1 and 2 is reached, the reactive power injection abruptly changes from supplying to consuming inductive reactive power, as it can be seen for six scenario days. The sudden change in the reactive power injection is caused by the cost-optimal maximization of the active power transfer across the cable. By consuming inductive reactive power, the PV array compensates reactive power locally. This allows for the maximum transfer of active power across the cable and therefore supports minimizing the reactive power transfer in the power grid.

Fig. 4 shows the line utilization at noon on the day of maximum solar irradiance (day 132) as determined by an AC power flow calculation. The right side shows the results for the design obtained with integrated AC power flow equations, while the left side shows the hypothetical line utilization for the active power injections of the CHP plant and PV array from the results of the single-node optimization. It can be seen that for the power flow results based on the single-node approach, branch 1 is heavily overloaded as indicated by the bright red color. For the CHP plant and PV array, active power and voltage magnitude are fixed to the values from the single-node optimization, while reactive power and phase angle are determined by the power flow. As the reactive power supply depends on the active power supply within the grid connection requirements, the PV array consumes almost its maximum inductive reactive power to keep its voltage magnitude. The CHP plant, however, is not able to inject any reactive power due to its lack of active power supply. In reality, the system would therefore lack reactive power. For the power flow calculation, we connected an external slack bus to bus 3 which consequently supplies the missing reactive power demand of the loads, the PV system and the feeders. In addition, the slack bus also provides the active power losses of the interconnecting branches which are not considered in the single-node approach.

Table III
OPTIMIZATION RESULTS: COMBINED HEAT AND POWER (CHP) PLANT SIZE (IN MW_{th}), PHOTOVOLTAIC (PV) ARRAY SIZE (IN MW_{peak}), DESIGN, OPERATIONAL AND TOTAL COSTS FOR THE SINGLE-NODE APPROACH AND WITH INTEGRATED AC POWER FLOW.

Parameter	Single-node	AC power flow
Size of CHP plant	5.15 MW	5.25 MW
Size of PV array	8 MW	5.81 MW
Design and fixed costs	1.01 M€/a	0.90 M€/a
Variable costs	4.90 M€/a	5.24 M€/a
Total costs	5.91 M€/a	6.14 M€/a

In brief, the line utilization based on the single-node approach optimization results in an overloaded branch and a deficit in reactive and active power supply. However, in the AC approach capacity limits are considered explicitly and thus upheld for all branches. Moreover, the reactive power for local voltage control can be fully supplied. The reason for the cable between buses 1 and 2 not being overloaded is the smaller size as well as the curtailment of the PV array. These results show that not considering grid restrictions of the power system can lead to significantly overloaded cables for the operation of MESs.

In summary, the results show that the impact of grid restrictions on MES design and operation can be substantial. MES design without consideration of power flow equations might result in suboptimal sizing of components and thus leads to economic losses. Even more importantly, the MES operation without explicit consideration of the power grid may lead to overloaded cables and possible power outages. Therefore, the integration of AC power flow equations in the design optimization is desirable. Furthermore, reactive power compensation for voltage stability can be indicated and planned.

IV. Conclusion

We present an integration of power grid restrictions into our MES optimization framework COMANDO. We demonstrate the effects of integrating AC power flow equations by comparing the resulting optimal design to the design resulting from the conventional single-node approach. In the considered case study, the single-node approach leads to an oversizing of the PV array of 38 %. This would result in a 56 % overrated cable during hours of high solar irradiance and thus the curtailment of the oversized PV array. Therefore, we recommend explicitly considering power flow equations in MES design optimization if grid restrictions may be a bottleneck.

Applying the COMANDO framework to design optimization of the power grid itself, e.g., by deciding where to lay new cables of which capacity or by sizing the interconnecting branches, would be a straight-forward extension of the illustrative case study considered here. In future work, the authors would like to extend COMANDO with similar, more advanced grid representations for gas and heating networks. This would enable design and operational optimization of power grids with coupled heat or gas grids on a campus or district level. Perspectively, for future power grids, the identification and placement of reactive power compensation systems for voltage stability of distribution networks is an important task that could be addressed within the proposed framework.

Bibliography

[1] P. Mancarella, "MES (multi-energy systems): An overview of concepts and evaluation models," *Energy*, vol. 65, pp. 1–17, 2014.

[2] S. Hilpert, C. Kaldemeyer, U. Krien, S. Günther, C. Wingenbach, and G. Plessmann, "The Open Energy Modelling Framework (oemof) - A new approach to facilitate open science in energy system modelling," *Energy Strategy Reviews*, vol. 22, pp. 16–25, 2018.

[3] M. Howells, H. Rogner, N. Strachan, C. Heaps, H. Huntington, S. Kypreos, A. Hughes, S. Silveira, J. DeCarolis, M. Bazillian, and A. Roehrl, "OSeMOSYS: The Open Source Energy Modeling System: An introduction to its ethos, structure and development," *Energy Policy*, vol. 39, no. 10, pp. 5850–5870, 2011, Sustainability of Biofuels.

[4] R. Loulou and M. Labriet, "ETSAP-TIAM: the TIMES integrated assessment model Part I: Model structure," *Computational Management Science*, vol. 5, pp. 7–40, 2008.

[5] A. S. Siddiqui, R. M. Firestone, S. Ghosh, M. Stadler, J. L. Edwards, and C. Marnay, "Distributed energy resources customer adoption modeling with combined heat and power applications," Ernest Orlando Lawrence Berkeley National Laboratory, Tech. Rep., 2003.

[6] P. Gabrielli, M. Gazzani, E. Martelli, and M. Mazzotti, "Optimal design of multi-energy systems with seasonal storage," *Applied Energy*, vol. 219, pp. 408–424, 2018.

[7] Z. Li and Y. Xu, "Optimal coordinated energy dispatch of a multi-energy microgrid in grid-connected and islanded modes," *Applied Energy*, vol. 210, pp. 974–986, 2018.

[8] H. W. Dommel and W. F. Tinney, "Optimal power flow solutions," *IEEE Transactions on Power Apparatus and Systems*, vol. PAS-87, no. 10, pp. 1866–1876, 1968.

[9] S. Frank and S. Rebennack, "An introduction to optimal power flow: Theory, formulation, and examples," *IIE Transactions*, vol. 48, no. 12, pp. 1172–1197, 2016.

[10] B. H. Bakken, H. I. Skjelbred, and O. Wolfgang, "eTransport: Investment planning in energy supply systems with multiple energy carriers," *Energy*, vol. 32, no. 9, pp. 1676–1689, 2007.

[11] S. Clegg and P. Mancarella, "Integrated electricity-heat-gas modelling and assessment, with applications to the Great Britain system. Part II: Transmission network analysis and low carbon technology and resilience case studies," *Energy*, vol. 184, pp. 191–203, 2019, Shaping Research in Gas-, Heat- and Electric-Energy Infrastructures.

[12] B. Morvaj, R. Evins, and J. Carmeliet, "Optimization framework for distributed energy systems with integrated electrical grid constraints," *Applied Energy*, vol. 171, pp. 296–313, 2016.

[13] R. D. Zimmerman, C. E. Murillo-Sánchez, and R. J. Thomas, "MATPOWER: Steady-state operations, planning, and analysis tools for power systems research and education," *IEEE Transactions on Power Systems*, vol. 26, no. 1, pp. 12–19, 2011.

[14] L. Thurner, A. Scheidler, F. Schafer, J. H. Menke, J. Dollichon, F. Meier, S. Meinecke, and M. Braun, "pandapower - an open source python tool for convenient modeling, analysis and optimization of electric power systems," *IEEE Transactions on Power Systems*, 2018.

[15] T. Brown, J. Hörsch, and D. Schlachtberger, "PyPSA: Python for power system analysis," *Journal of Open Research Software*, vol. 6, no. 4, 2018.

[16] M. Langiu, D. Y. Shu, F. J. Baader, D. Hering, U. Bau, A. Xhonneux, D. Müller, A. Bardow, A. Mitsos, and M. Dahmen, "COMANDO: A next-generation open-source framework for energy systems optimization," *Computers & Chemical Engineering*, vol. 152, p. 107366, 2021.

[17] Z. Yang, K. Xie, J. Yu, H. Zhong, N. Zhang, and Q. Xia, "A general formulation of linear power flow models: Basic theory and error analysis," *IEEE Transactions on Power Systems*, vol. 34, no. 2, pp. 1315–1324, 2019.

[18] ETSO, "Definitions of transfer capacities in liberalised electricity markets," *Final Report*, April 2001.

[19] J. Zhu, *Optimization of Power System Operation*, 2nd ed. Hoboken, NJ, USA: John Wiley & Sons, January 2015.

[20] G. Andersson, "Modelling and Analysis of Electric Power Systems," *Lecture 227-0526-00, ITET ETH Zürich, Zürich*, 2008.

[21] Consentec GmbH, "Konventionelle Mindesterzeugung - Einordnung, aktueller Stand und perspektivische Behandlung," Availabe at http://www.consentec.de/publikationen/studien (accessed on 01/12/2021).

[22] K. Turitsyn, P. Sulc, S. Backhaus, and M. Chertkov, "Options for control of reactive power by distributed photovoltaic generators," *Proceedings of the IEEE*, vol. 99, no. 6, pp. 1063–1073, 2011.

[23] S. Pfenninger and I. Staffell, "Renewables.Ninja," Available at https://www.renewables.ninja (accessed on 14/11/2021).

[24] S. Pfenninger and I. Staffell, "Long-term patterns of European PV output using 30 years of validated hourly reanalysis and satellite data," *Energy*, vol. 114, pp. 1251–1265, 2016.

[25] A. Wächter and L. T. Biegler, "On the implementation of an interior-point filter line-search algorithm for large-scale nonlinear programming," *Mathematical Programming*, vol. 106, no. 1, pp. 25–57, apr 2005.